Supporting information for

High-Performance Diluted Nickel Nanoclusters Decorating Ruthenium Nanowires for pH-Universal Overall Water Splitting

Ting Zhu[a,b,#], Shangheng Liu[a,#], Bin Huang[b,#], Qi Shao[a,], Man Wang[c], Fan Li[d], Xinyue Tan[a], Yecan Pi[a], Shih-Chang Weng[e], Bolong Huang[f,*], Zhiwei Hu[g], Jianbo Wu[d], Yong Qian[b], and Xiaoqing Huang[a,h,*]*

[a]T. Zhu, S. Liu, Dr. Q. Shao, X. Tan, Dr. Y. Pi, Prof. X. Huang

[a]College of Chemistry, Chemical Engineering and Materials Science, Soochow University, Jiangsu 215123, P. R. China.

[b]T. Zhu, Dr. Bin. Huang, Prof. Y. Qian

[b]Jiangxi Province Key Laboratory of Polymer Micro/Nano Manufacturing and Devices, East China University of Technology, Nanchang, Jiangxi 330013, P. R. China

[c]Dr. M. Wang

[c]Guangdong Provincial Key Laboratory of Energy Materials for Electric Power, Southern University of Science and Technology, Shenzhen 518055, P. R. China.

[d]F. Li, Prof. J. Wu

[d]School of Materials Science and Engineering, Shanghai Jiao Tong University, Shanghai, 200240, P. R. China.

[e]Dr. S. Weng

[e]National Synchrotron Radiation Research Center, Hsinchu, 30076, Taiwan.

[f]Prof. Bolong. Huang

[f]Department of Applied Biology and Chemical Technology, The Hong Kong Polytechnic University, Hung Hom, Kowloon, Hong Kong SAR.

[g]Prof. Z. Hu

[g]Max-Planck-Institute for Chemical Physics of Solids, Nöthnitzer Street, 4001187, Dresden, Germany.

[h]Prof. X. Huang

[h]College of Chemistry and Chemical Engineering, Xiamen University, Xiamen, 361005, P. R. China.

[#]These authors contributed equally.

Email: qshao@suda.edu.cn; bhuang@polyu.edu.hk; hxq006@xmu.edu.cn

S1. Experimental Section

1.1 Chemicals

Potassium aquapenachloro-ruthenate (III) ($K_2RuCl_5 \cdot H_2O$) and Nafion were purchased from Sigma-Aldrich. Polyvinyl pyrrolidone (PVP, MW = 58000, AR) was obtained from J&K Scientific Ltd. Sodium formate (HCOONa) was purchased from Aladdin-reagent Inc. Nickel (II) formate dehydrate ($Ni(HCOO)_2 \cdot 2H_2O$) was purchased from Alfa Aesar. Potassium hydroxide (KOH, AR, ≥ 85%), ethanol (C_2H_6O), isopropanol (C_3H_8O), acetone (C_3H_6O) and sulfuric acid (H_2SO_4) were purchased from Sinopharm Chemical Reagent Co. Ltd. (Shanghai, China). Vulcan XC-72 R carbon black was purchased from Caebot. Commercial Pt/C (20 wt%) and commercial Ir/C (20 wt%) were purchased from Johnson Matthey (JM) Corporation. All the chemicals were used as received without further purification. The ultra-pure water (18 MΩ cm^{-1}, Aqua Solutions) was used in all experiments.

1.2 Synthesis of Ni-Ru NWs and Ru NWs

In a typical preparation of Ni-Ru NWs, $K_2RuCl_5 \cdot H_2O$ (9.4 mg), $Ni(HCOO)_2 \cdot 2H_2O$ (4.6 mg), PVP (40 mg) and H_2O (10 mL) were added into a 20 mL Teflon-lined stainless-steel autoclave. The mixture was ultrasonicated for around 30 min. The resulting homogeneous mixture was then heated at 200 °C for 24 h before it cooled down to room temperature. The resulting colloidal product was collected by centrifugation and washed with a mixture of ethanol (1 mL) and acetone (8 mL). The preparation of Ru NWs was similar to that of Ni-Ru NWs except that $Ni(HCOO)_2 \cdot 2H_2O$ (4.6 mg) was replaced by HCOONa (1.7 mg).

1.3 Synthesis of $Ni_{cluster}$-Ru NWs

In a typical preparation of $Ni_{cluster}$-Ru NWs, the Ni-Ru NWs were transferred into nitrogen-saturated 0.5 M H_2SO_4. The NWs was magnetically stirred under 500 r s^{-1} for 12 hours to remove the Ni species on the surface. The resulting products were collected by centrifugation and washed by water with several times.

1.4 Preparations of supported catalysts

To prepare the catalysts, nanowires were loaded on carbon powder (VXC-72, Carbot) in 10 mL ethanol and sonicated for 0.5 h to deposit NWs on carbon. The products were separated by centrifugation and washed with ethanol/acetone three times, and finally kept in the vacuum drying oven under 60 °C for 12 h. And then annealed in air at 250 °C for 1 h.

1.5 Characterization

The samples were prepared by dropping cyclohexane or ethanol dispersion of samples onto carbon-coated copper TEM grids using pipettes and dried under ambient conditions. Low-magnification transmission electron microscopy (TEM) was conducted on a HITACHI HT7700 transmission electron microscope at an accelerating voltage of 120 kV. Atomic resolution aberration-corrected HAADF-STEM was conducted on JEM-ARM300F Grand ARM Transmission Electron Microscope. Powder X-ray Diffraction (PXRD) pattern was collected on X'Pert-Pro MPD diffractometer (Netherlands PANalytical) with a Cu Kα X-ray source (λ = 1.540598 Å). XAS data were collected at the TLS-07A beamline of the National Synchrotron Radiation Research Center (NSRRC, Hsinchu, Taiwan). The EXAFS data were processed according to the standard procedures using the ATHENA module implemented in the "IFEFFIT software packages" in the method section of the revised manuscript.[1] The concentration of catalysts was determined by the inductively coupled plasma optical emission spectrometer (Varian 710-ES). X-ray photoelectron spectra (XPS) was collected with an SSI S-Probe XPS Spectrometer. TGA was performed on SII TG/DTA 6300 thermogravimetric analyzer over a temperature range of 25-900 °C at a heating rate of 10 °C min^{-1} in oxygen atmosphere. ICP-OES was performed on Agilent 5110. The hydrogen was analyzed by gas chromatography (GC 9860). Other characterizations were collected by the same instruments mentioned in our previous studies.[2-4]

1.6 Electrochemical measurements

For all the electrochemical tests, a three-electrode system was used to conduct the electrochemical measurements at an electrochemical workstation (CHI 660E). The catalyst

(2.0 mg) was dispersed in 390 μL water-ethanol solution (3:1, v/v) with 10 μL 5 wt% Nafion by syndicating for 1 h to form a homogeneous ink. The working electrode was fabricated by casting 10 μL catalyst ink onto a glassy carbon electrode (GCE) (diameter: 5 mm, area: 0.196 cm^2). The mass loading of the catalyst was 0.25 mg cm^{-2}. A graphite rod and a saturated calomel electrode (SCE) were used as the counter electrode and reference electrode, respectively. The reference was calibrated with respect to the reversible hydrogen electrode (RHE). Linear sweep voltammetry (LSV) was carried out at 5 mV s^{-1} at room temperature. The electrochemical active surface area (ECSA) was determined by electrochemical double-layer capacitance (C_{dl}) measurements on cyclic voltammetry (CV) at room temperature from 20 mV s^{-1} to 200 mV s^{-1}. Electrochemical impedance spectroscopy (EIS) was collected at the overpotential of 10 mV with the frequency range from 0.01 to 100 kHz. For comparison, the commercial Pt/C was examined in all tests under the same conditions.

1.7 Computational details

The simplified rotationally invariant DFT+U calculations within CASTEP code have been selected to investigate the electronic and energetic properties.[5, 6] We choose the algorithm of Broyden-Fletcher-Goldfarb-Shannon (BFGS) for all the ground state geometry optimization in this work. The PBE exchange-correlation functional is selected for DFT+U calculations. To improve the convergence quality of the transition metal systems for $Ni_{cluster}$-Ru, the ensemble DFT (EDFT) by Marzari et al. has been applied during electronic-minimization process.[7] The cutoff energy of plane-wave basis sets for total energy calculations has been set to 750 eV.

The substrate Ru-surface model was built based on the bulk hcp-Ru crystal, where the surface system has been built with 10-layer thickness. The surface Ni cluster has been constructed from the unit cell of fcc-Ni with a size of 15 atoms and anchored on the Ru surfaces. To ensure sufficient space for all the geometry optimization and adsorption of intermediates, we set the vacuum space of 15 Å along the z-axis. Considering the DFT computational cost, the Monkhost-Pack reciprocal space integration was performed using Gamma-center-off special

k-points with a mesh of 2×2×2, which was guided by the initial convergence test.[8] The overall total convergence settings have been set that the total energy for each step should be less than 5.0×10^{-7} eV per atom while the Hellmann-Feynman forces on the atom should not exceed 0.001 eV/Å.

Through the OPIUM code in the Kleinman-Bylander projector form, the norm-conserving pseudopotentials of Ru, Ni, O, and H are generated.[9] Meanwhile, to treat the mixed valence Ru and Ni spin-orbital coupling effect, the non-linear partial core correction and a scalar relativistic averaging scheme are applied.[10, 11] The projector-based (4d, 5s, 5p), (3d, 4s, 4p), (2s, 2p), and (1s) states have been chosen to reflect the valence states of Ru, Ni, O, and H atoms, respectively. The RRKJ method is chosen for the optimization of the pseudopotentials.[12]

1.8 Active Sites Calculations

The number of active sites (n) can be qualified based on the underpotential deposition (UPD) copper stripping charge (Q_{Cu}, $Cu_{UPD} \rightarrow Cu^{2+} + 2e^-$) with the following formula:

$n = Q_{Cu} / 2F$,

where F is the Faraday constant (C mol^{-1}).[13]

1.9 Turnover Frequency (TOF) Calculations

TOF was calculated using the following formula:

$TOF = I / (2Fn)$,

where I is the current (A) during the linear sweep measurement, F is the Faraday constant (C mol^{-1}), n is the active sites (mol).[13]

S2. Figures:

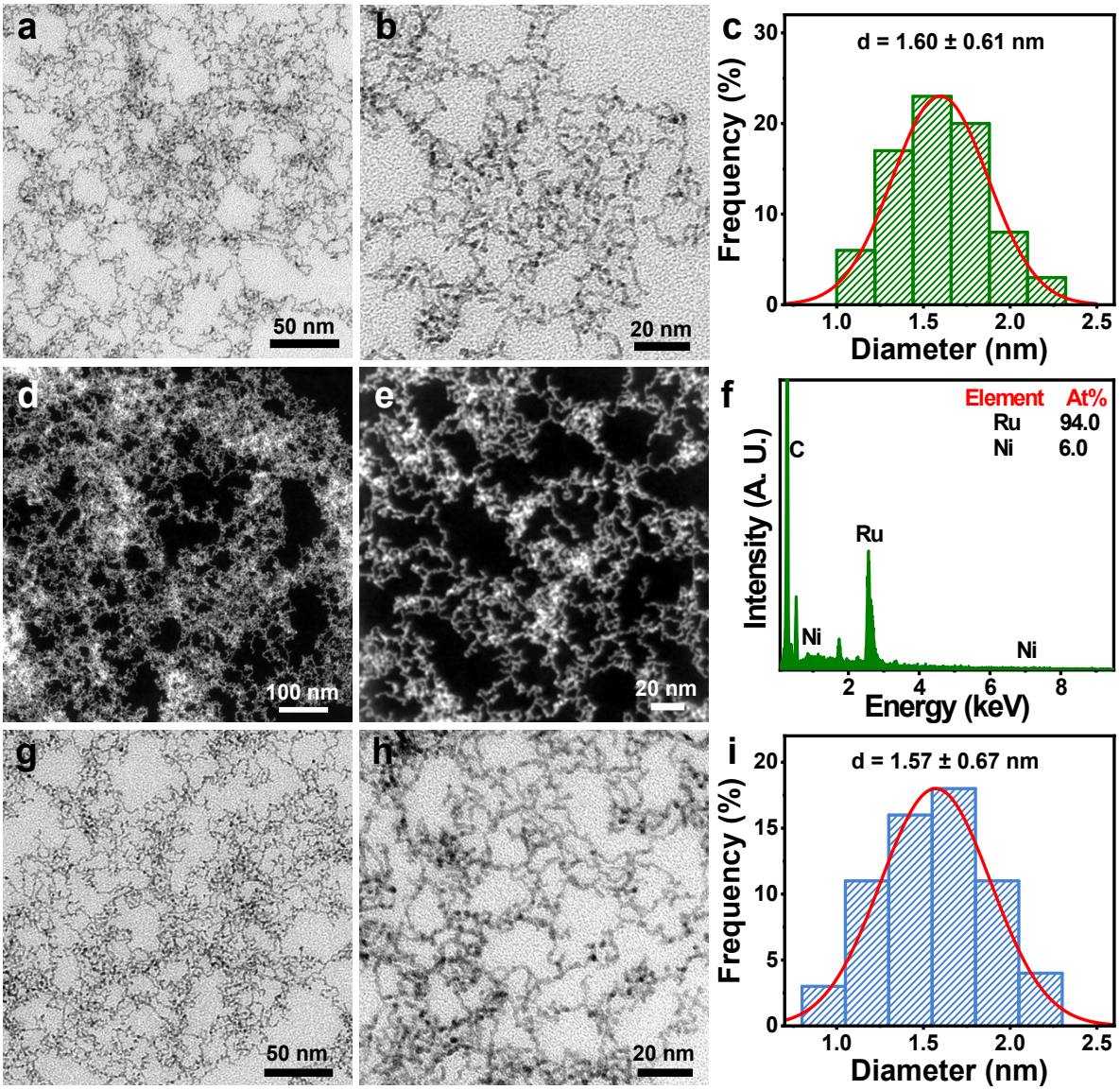

Fig. S1. (**a, b**) TEM images, (**c**) corresponding diameter histogram, (**d, e**) HAADF-STEM images and (**f**) EDS analysis of $Ni_{cluster}$-Ru NWs. (**g, h**) TEM images, (**i**) corresponding diameter histogram of Ru NWs.

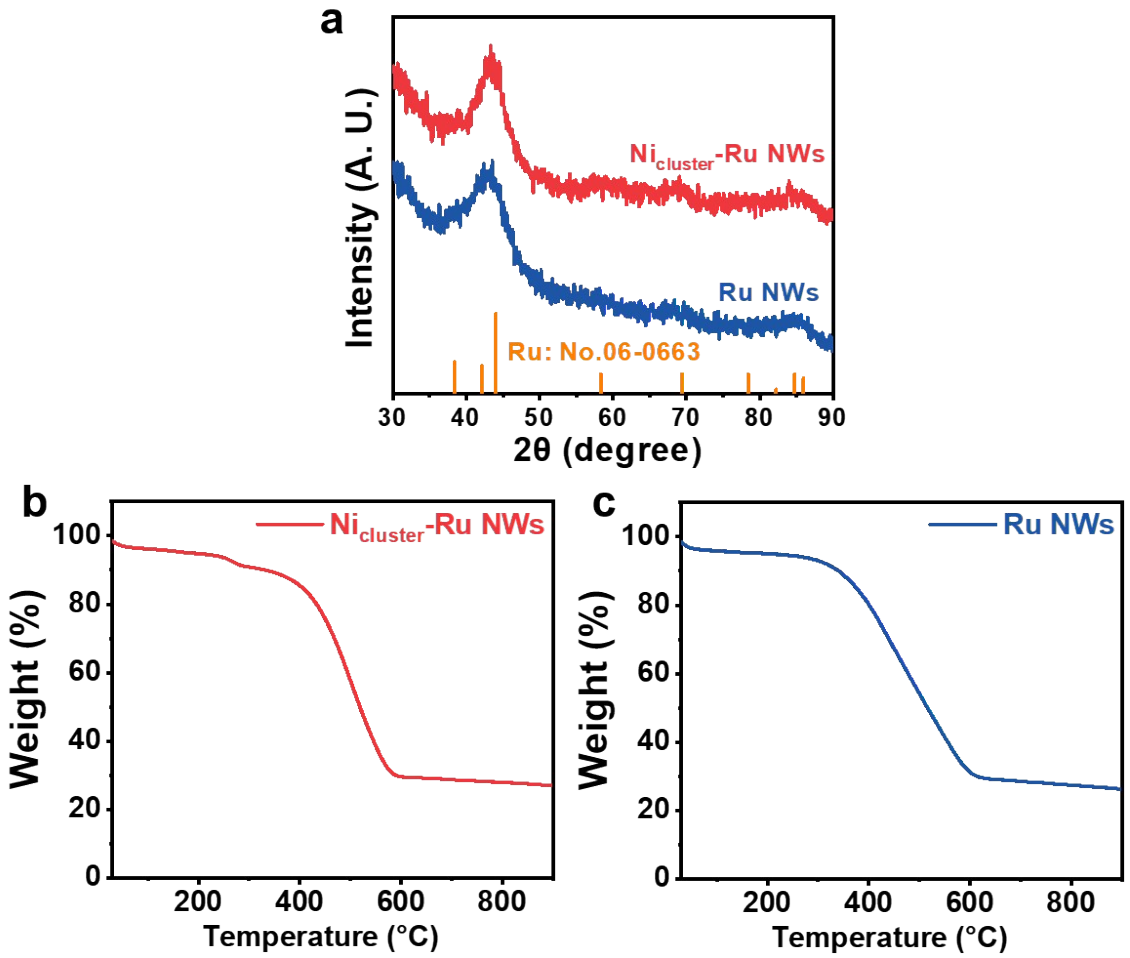

1

2 **Fig. S2.** (**a**) XRD patterns of $Ni_{cluster}$-Ru NWs and Ru NWs. TGA curves of (**b**) $Ni_{cluster}$-Ru
3 NWs and (**c**) Ru NWs.

1 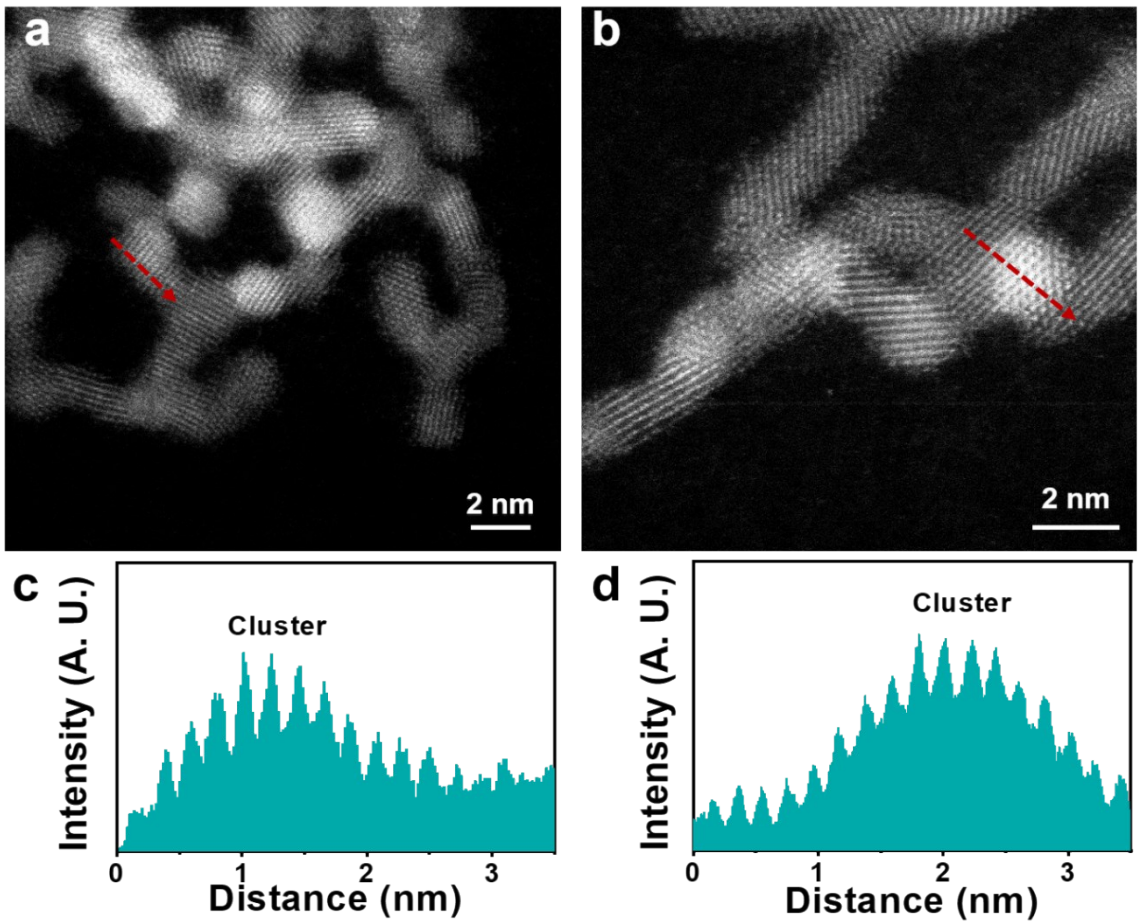

2 **Fig. S3.** (**a, b**) HRTEM images and (**c, d**) corresponding line scanning profiles $Ni_{cluster}$-Ru
3 NWs.

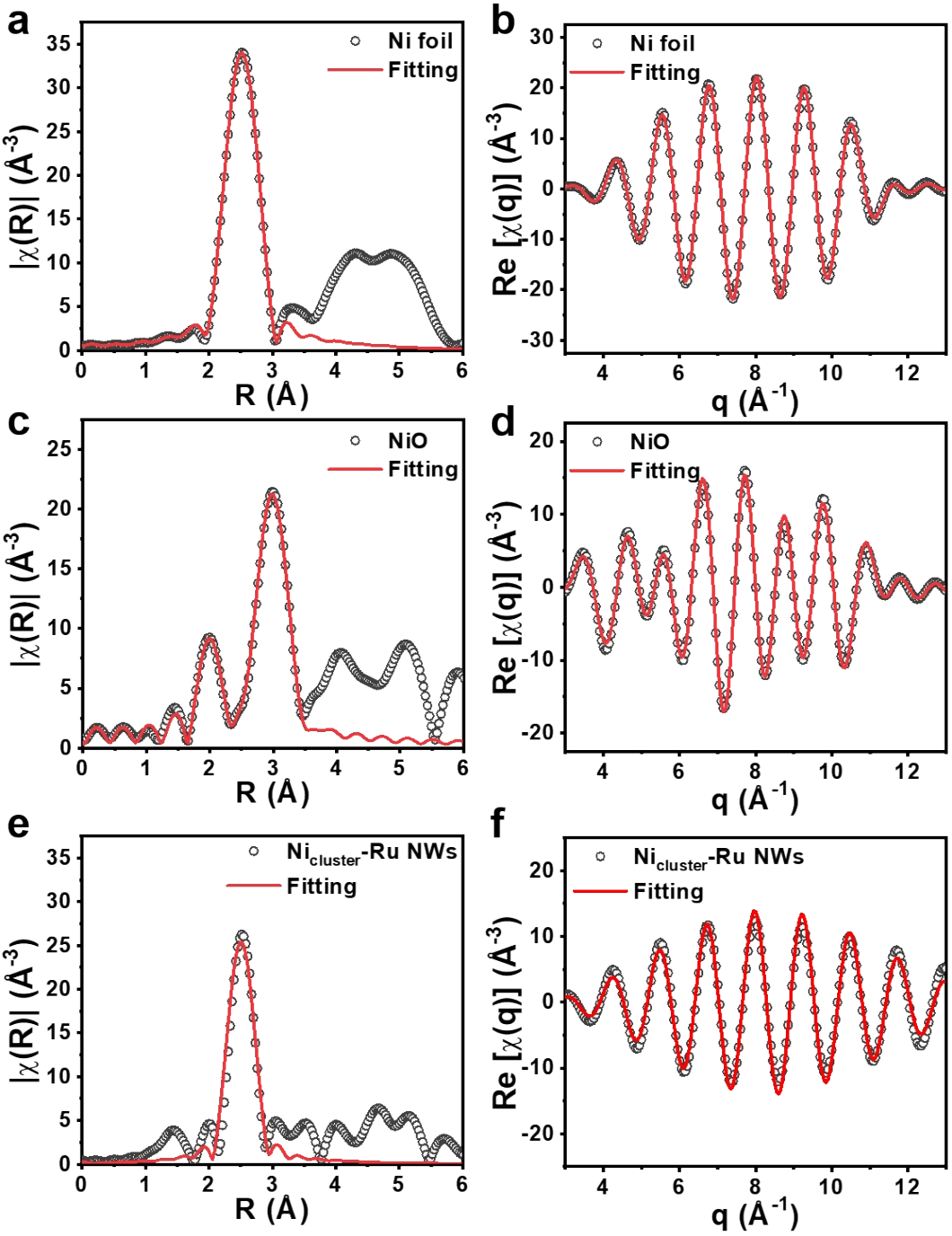

1

2 **Fig. S4.** (**a, c, e**) R space and (**b, d, f**) inverse FT-EXAFS fitting results of Ni K-edge for (**a,**

3 **b**) Ni foil, (**c, d**) NiO and (**e, f**) $Ni_{cluster}$-Ru NWs.

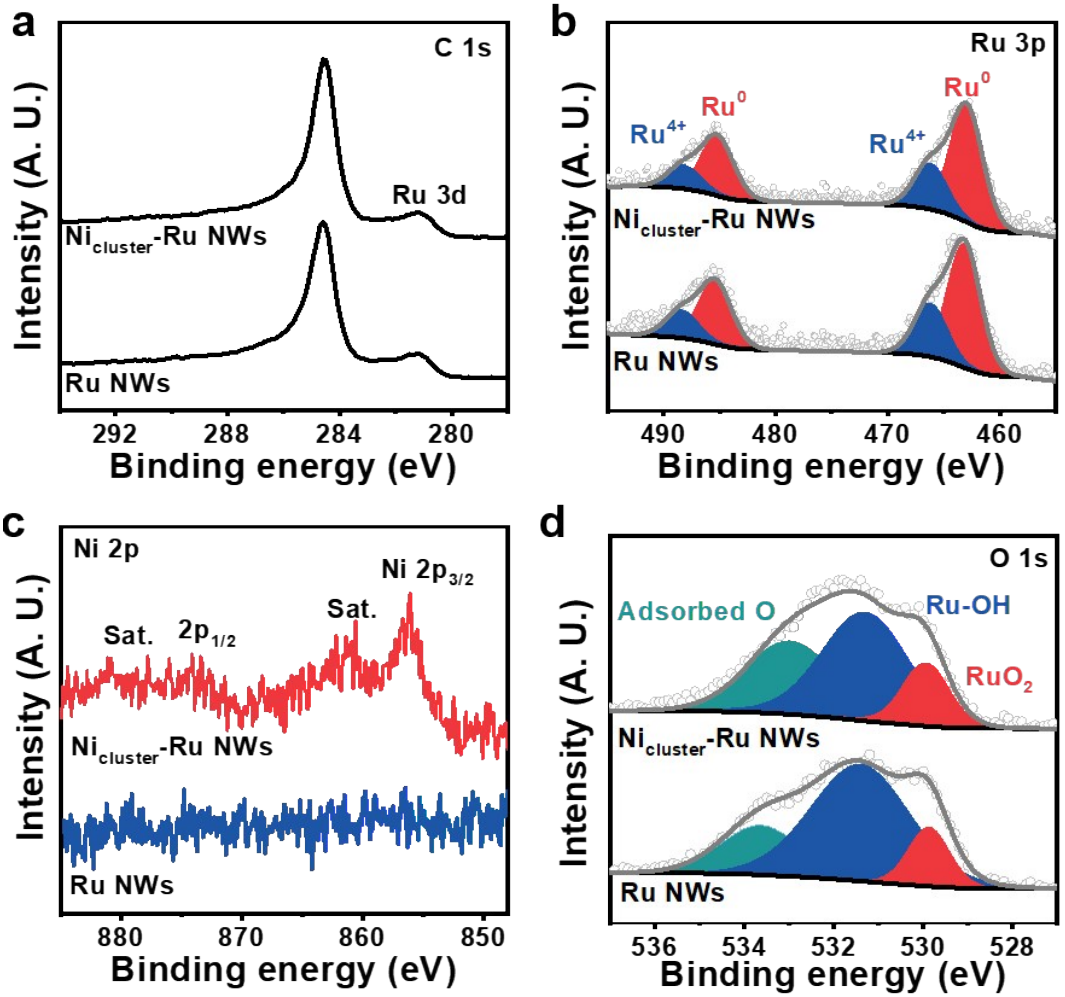

Fig. S5. (**a**) C 1s, (**b**) Ru 3p, (**c**) Ni 2p and (**d**) O 1s XPS spectra of $Ni_{cluster}$-Ru NWs and Ru NWs.

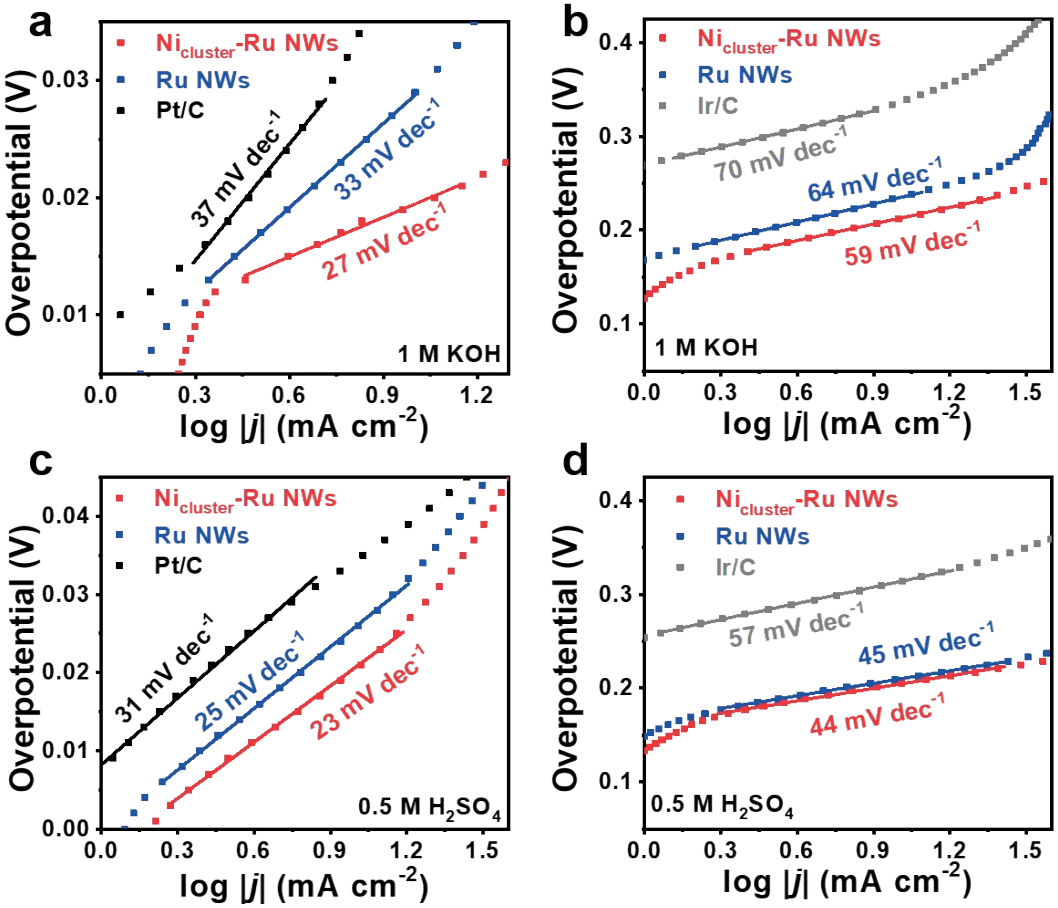

Fig. S6. Tafel slopes for (**a, c**) HER and (**b, d**) OER of $Ni_{cluster}$-Ru NWs, Ru NWs, Pt/C and Ir/C in (**a, b**) 1 M KOH and (**c, d**) 0.5 M H_2SO_4, respectively.

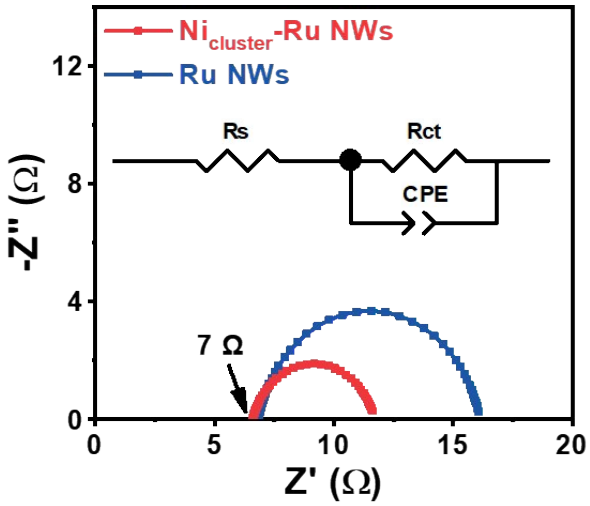

Fig. S7. EIS curves of $Ni_{cluster}$-Ru NWs and Ru NWs for HER in 1 M KOH.

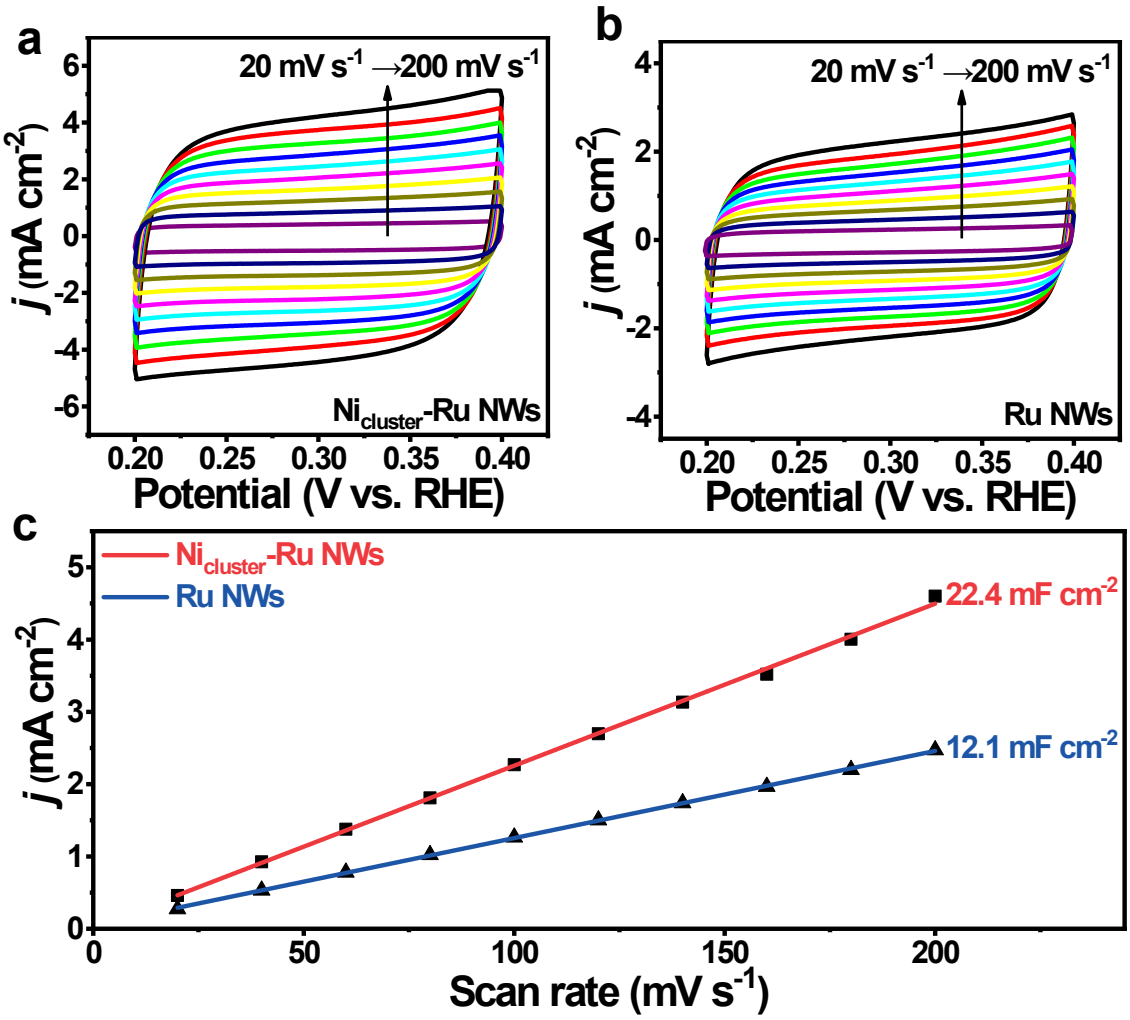

Fig. S8. (**a, b**) Cyclic voltammogram curves and (**c**) their corresponding plots of the charging current density against scan rates of (**a**) $Ni_{cluster}$-Ru NWs and (**b**) Ru NWs in a potential region of 0.2 ~ 0.4 V vs. RHE.

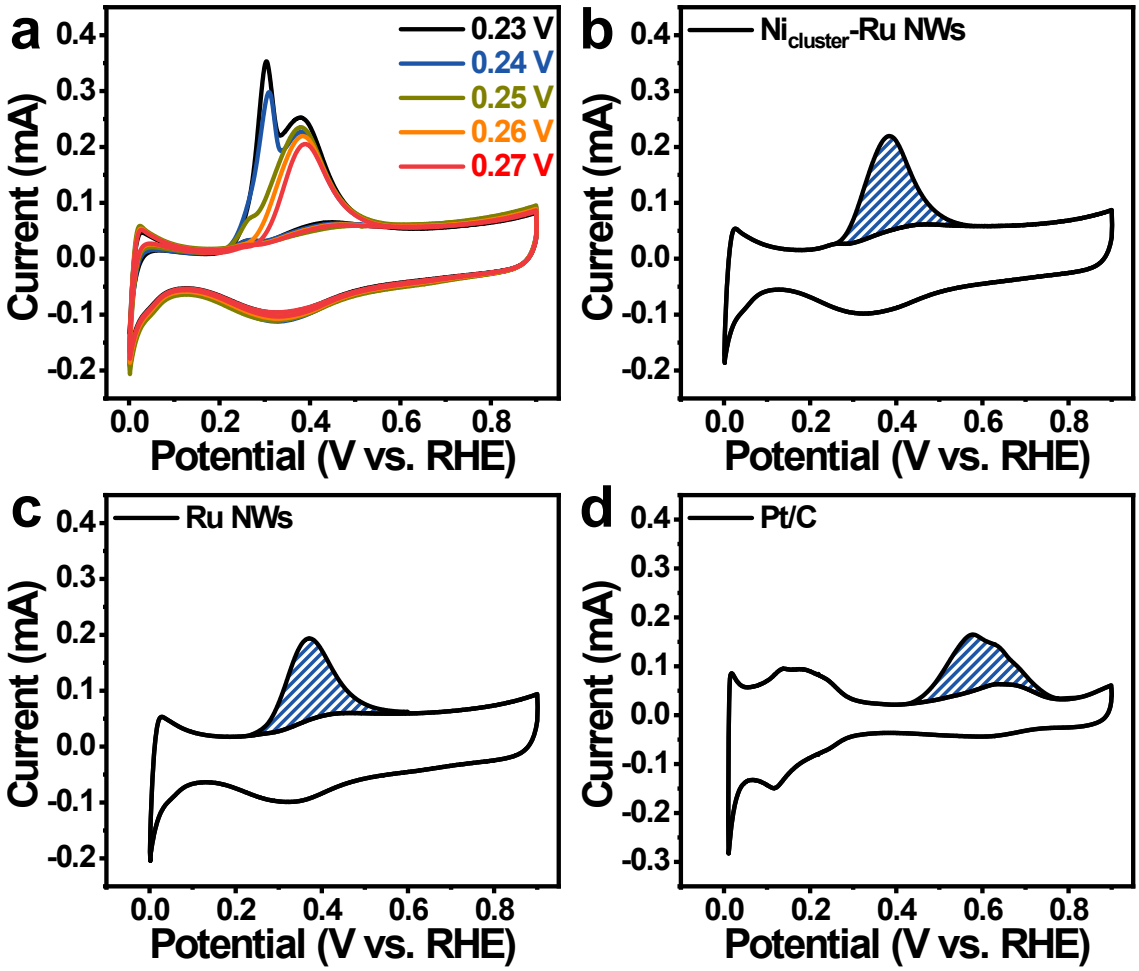

Fig. S9. (**a**) Copper UPD in 0.5 M H_2SO_4 + 5 mM $CuSO_4$ on $Ni_{cluster}$-Ru NWs polarized from 0.23 V - 0.27 V (vs. RHE) to form the UPD layers. Copper UPD in 0.5 M H_2SO_4 + 5 mM $CuSO_4$ on (**b**) $Ni_{cluster}$-Ru NWs, (**c**) Ru NWs and (**d**) Pt/C. The electrodes were polarized at 0.26 V (vs. RHE) for 100 s to form the UPD layer.

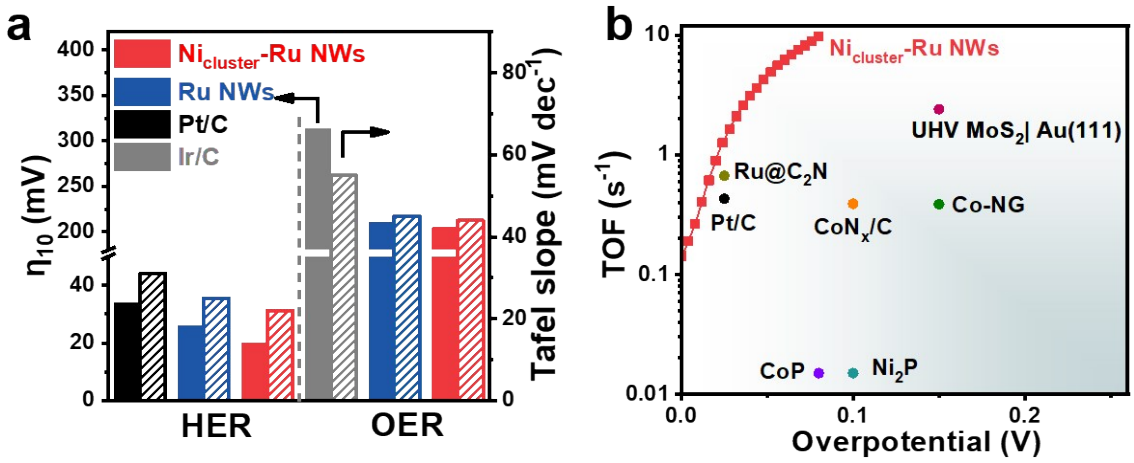

Fig. S10. (**a**) Overpotentials at 10 mA cm^{-2} and Tafel plots of Ni$_{cluster}$-Ru NWs, Ru NWs, Pt/C and Ir/C in 0.5 M H_2SO_4. (**b**) TOF values of Ni$_{cluster}$-Ru NWs, Ru NWs, Pt/C and previously reported catalysts for HER in 0.5 M H_2SO_4.

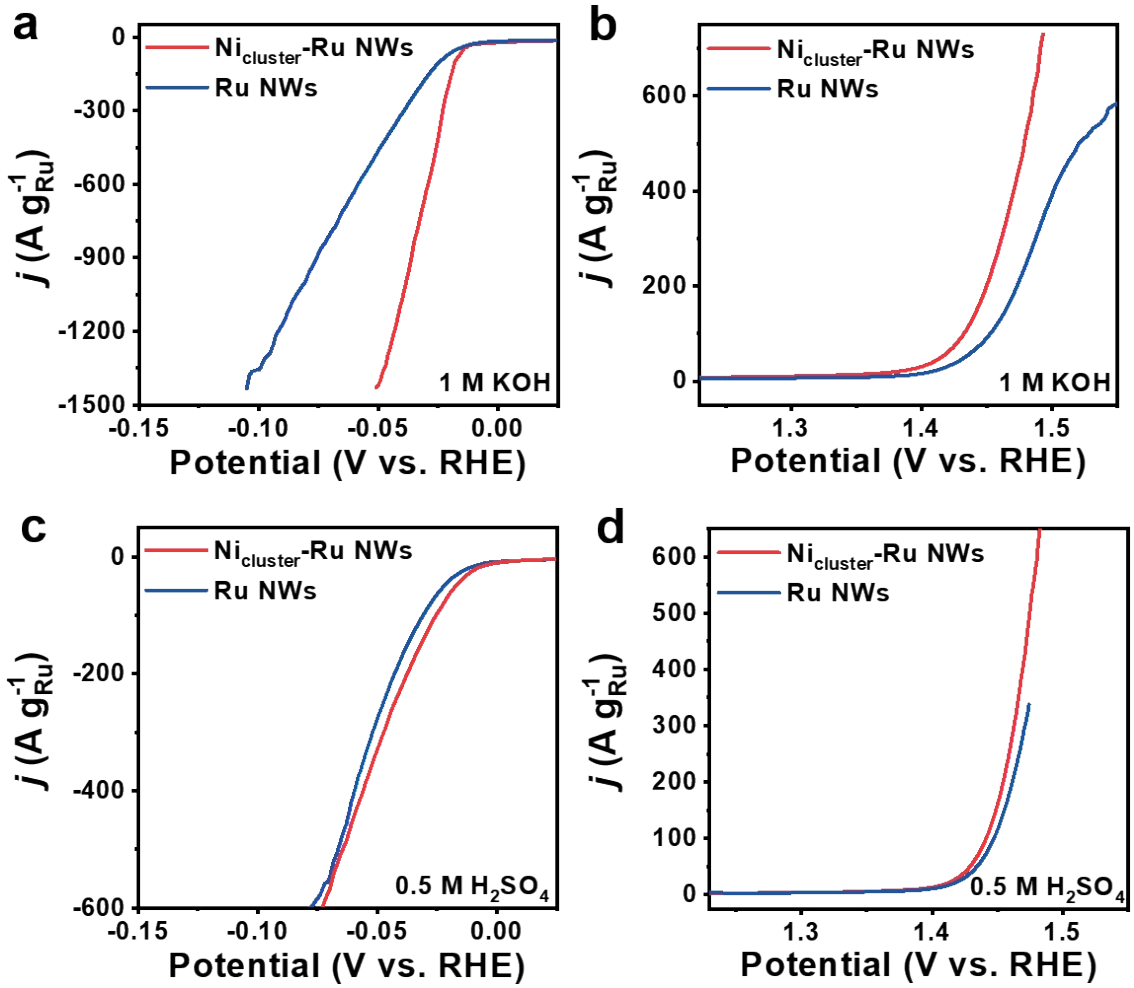

Fig. S11. Ru mass normalized (**a, c**) HER and (**b, d**) OER polarization curves of $Ni_{cluster}$-Ru NWs and Ru NWs in (**a, b**) 1 M KOH and (**c, d**) 0.5 M H_2SO_4.

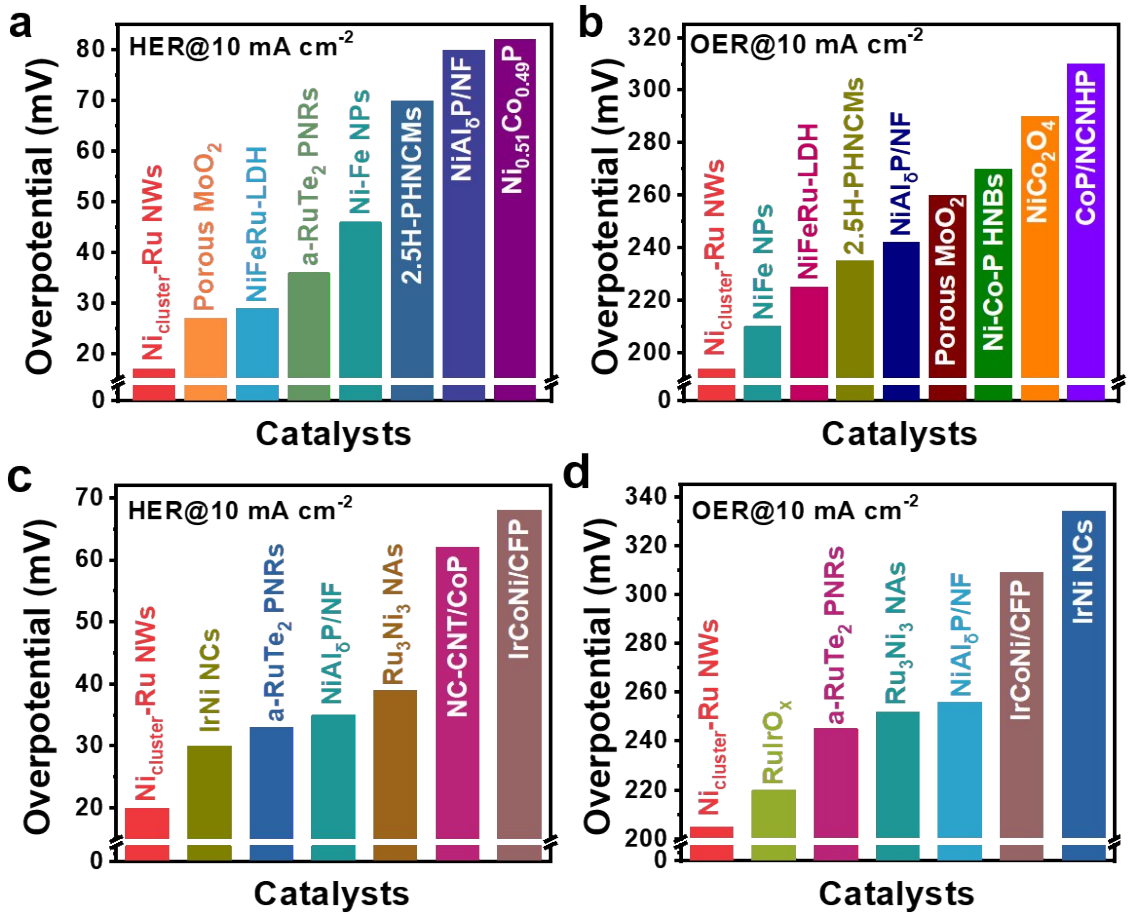

Fig. S12. Comparison of the overpotentials at 10 mA cm^{-2} among $Ni_{cluster}$-Ru NWs and available reported catalysts towards (**a, c**) HER and (**b, d**) OER in (**a, b**) 1 M KOH and (**c, d**) 0.5 M H_2SO_4, respectively (**Table S4**).

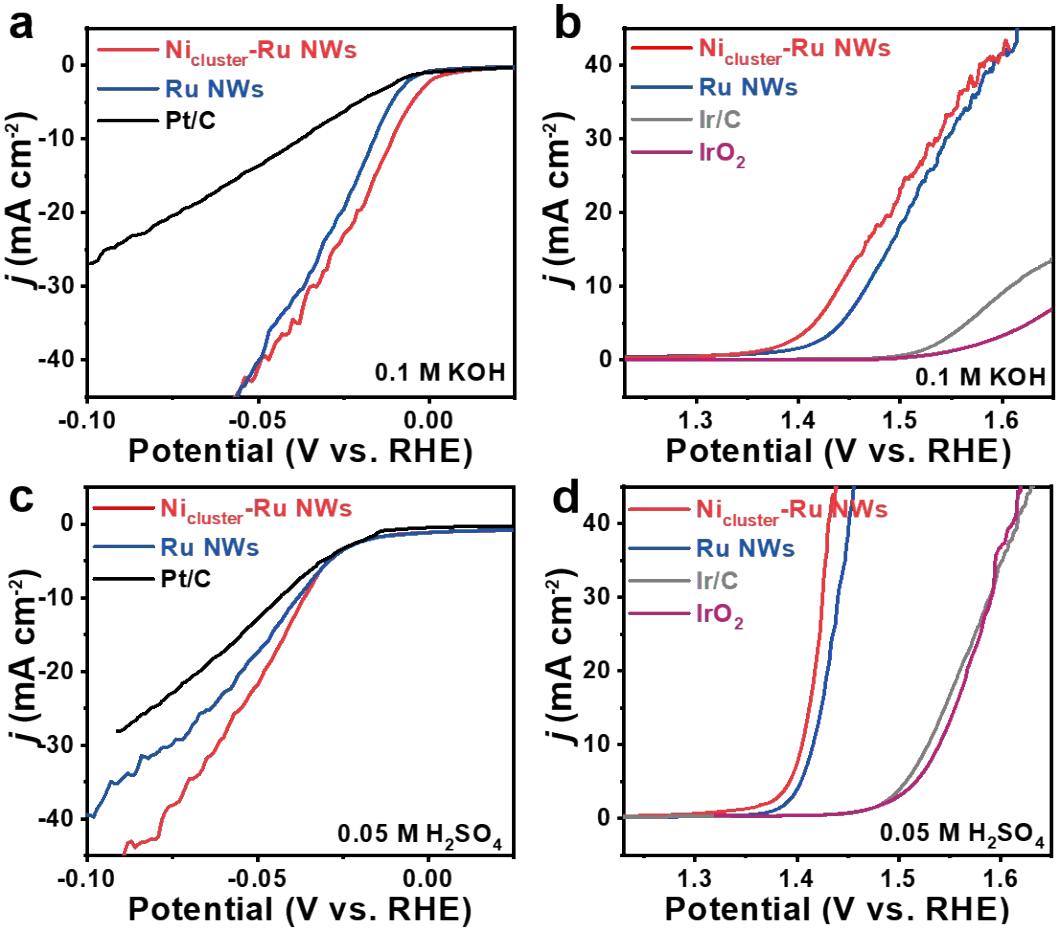

Fig. S13. Polarization curves for (**a, c**) HER and (**b, d**) OER of $Ni_{cluster}$-Ru NWs, Ru NWs, Ir/C, IrO_2 and Pt/C in (**a, b**) 0.1 M KOH and (**c, d**) 0.05 M H_2SO_4.

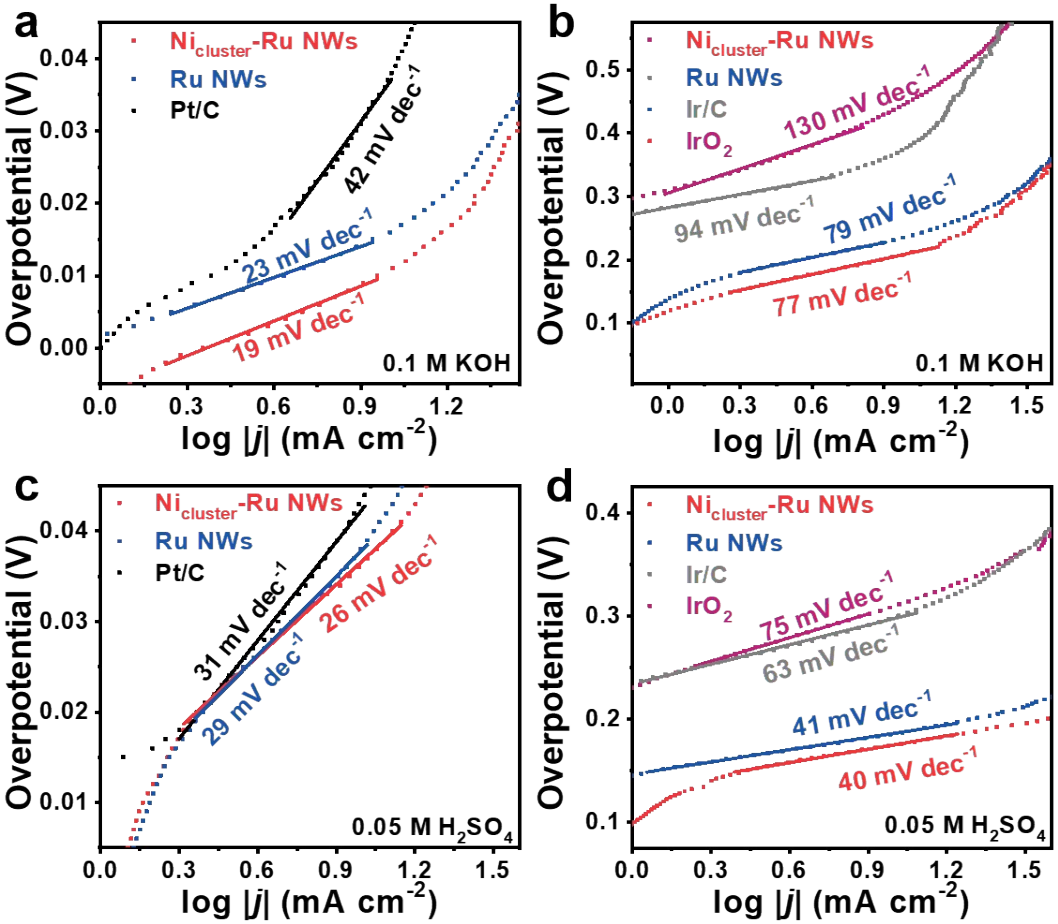

Fig. S14. Tafel slopes for (**a, c**) HER and (**b, d**) OER of $Ni_{cluster}$-Ru NWs, Ru NWs, Ir/C, IrO_2 and Pt/C in (**a, b**) 0.1 M KOH and **(c, d**) 0.05 M H_2SO_4.

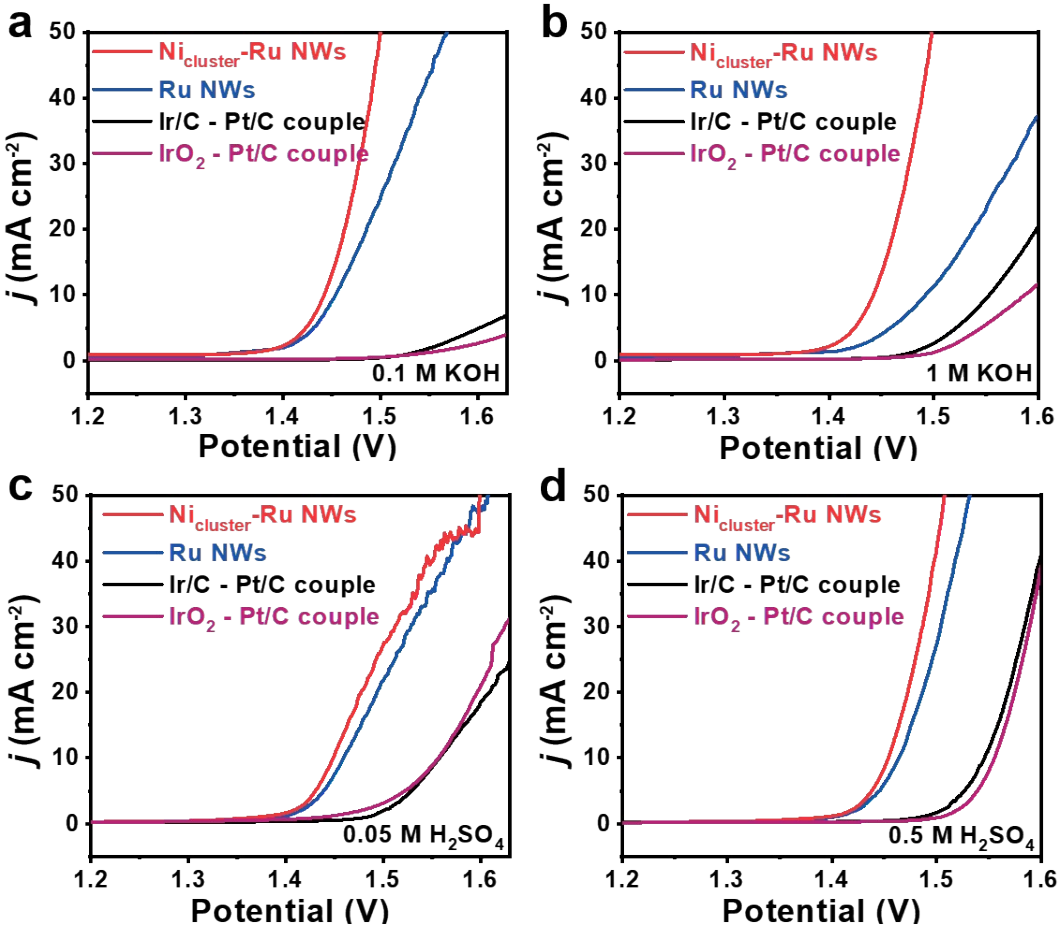

Fig. S15. Polarization curves for overall water splitting of $Ni_{cluster}$-Ru NWs, Ru NWs, Ir/C-Pt/C couple and IrO_2-Pt/C couple in (**a**) 0.1 M KOH, (**b**) 1 M KOH, (**c**) 0.05 M H_2SO_4 and (**d**) 0.5 M H_2SO_4.

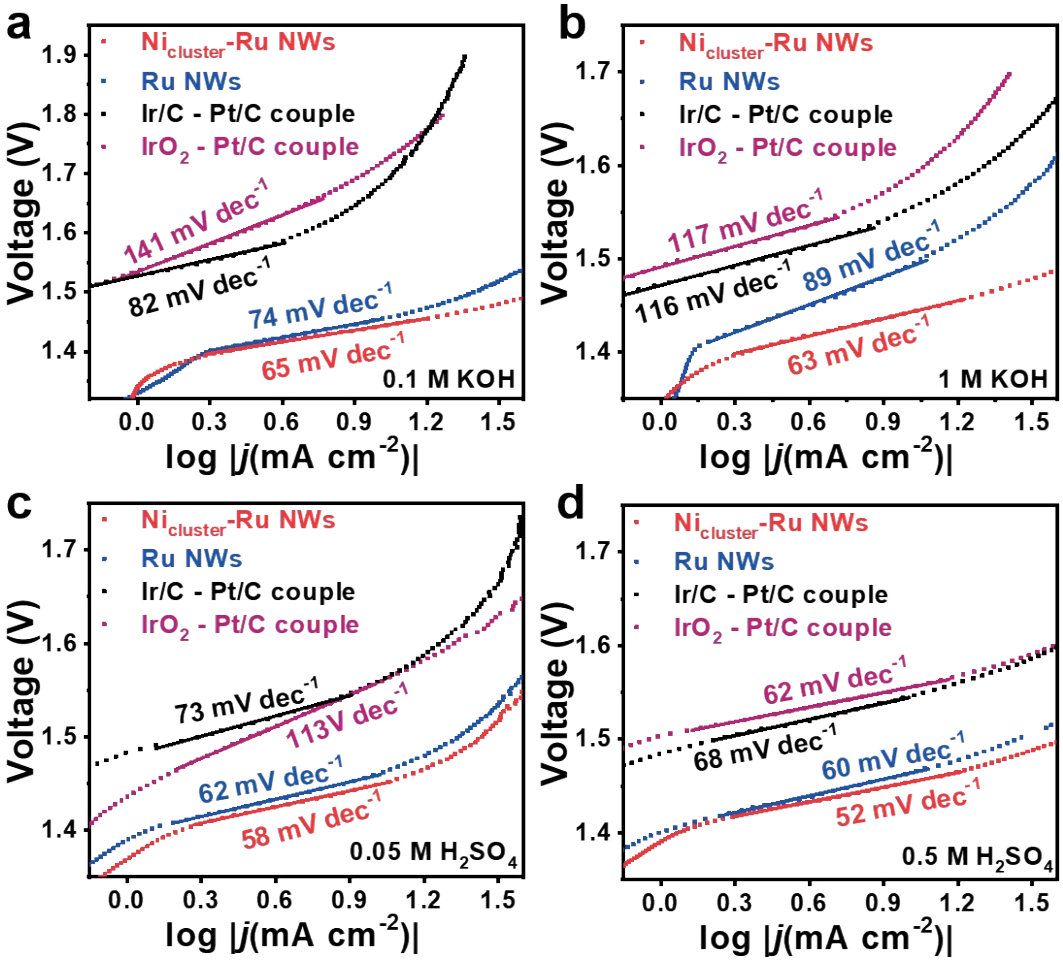

Fig. S16. Tafel slopes for overall water splitting of $Ni_{cluster}$-Ru NWs, Ru NWs, Ir/C-Pt/C couple and IrO_2-Pt/C couple in (**a**) 0.1 M KOH, (**b**) 1 M KOH, (**c**) 0.05 M H_2SO_4 and (**d**) 0.5 M H_2SO_4.

1 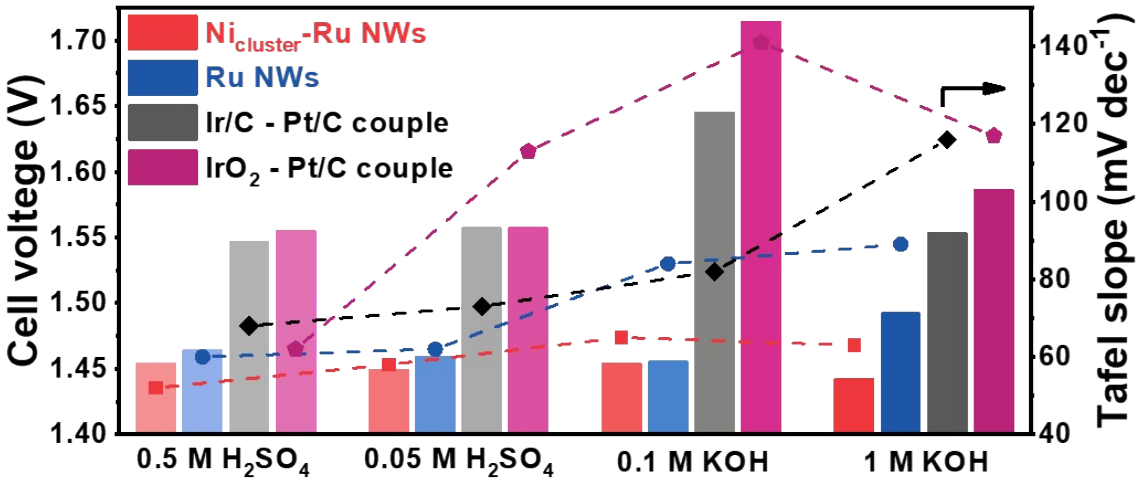

2 **Fig. S17.** The cell voltages at 10 mA cm^{-2} and Tafel plots of Ni$_{cluster}$-Ru NWs, Ru NWs, Ir/C-
3 Pt/C couple and IrO_2-Pt/C couple of overall water splitting under different pH conditions.

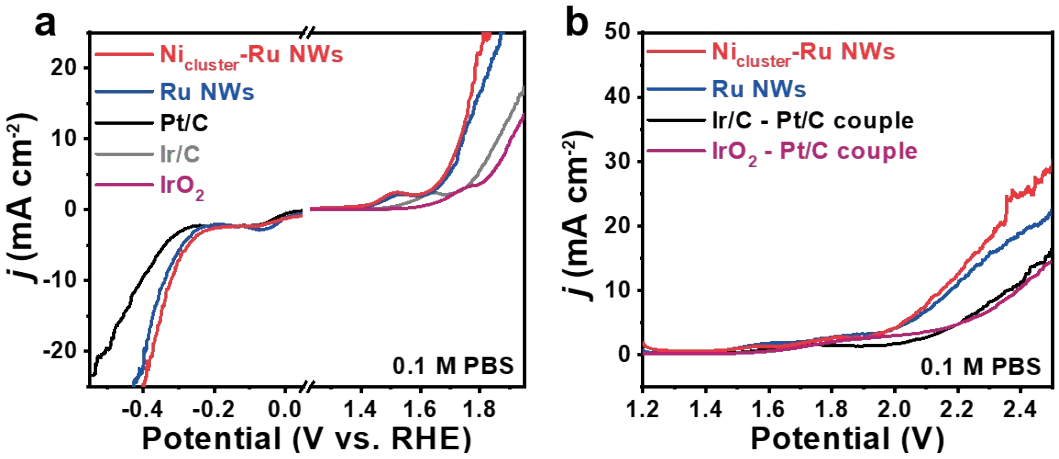

Fig. S18. (**a**) HER and OER polarization curves of $Ni_{cluster}$-Ru NWs, Ru NWs, Pt/C, Ir/C and IrO_2 in 0.1 M PBS. (**b**) Polarization curves for overall water splitting of $Ni_{cluster}$-Ru NWs, Ru NWs, Ir/C-Pt/C couple and IrO_2-Pt/C couple in 0.1 M PBS.

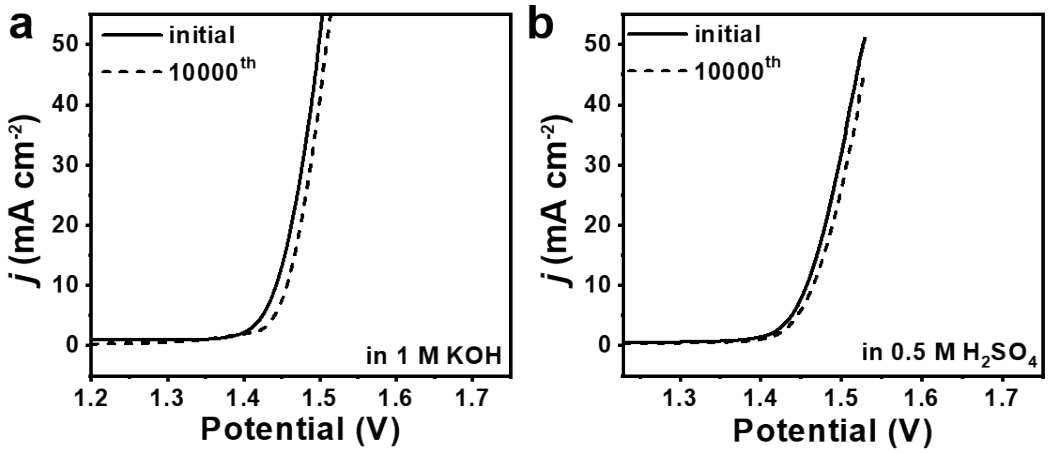

1

2 **Fig. S19.** The polarization curves of $Ni_{cluster}$-Ru NWs measured before and after different
3 cycles in (**a**) 1 M KOH and (**b**) 0.5 M H_2SO_4, respectively (CV scan range from 1.23 V to 1.6
4 V).

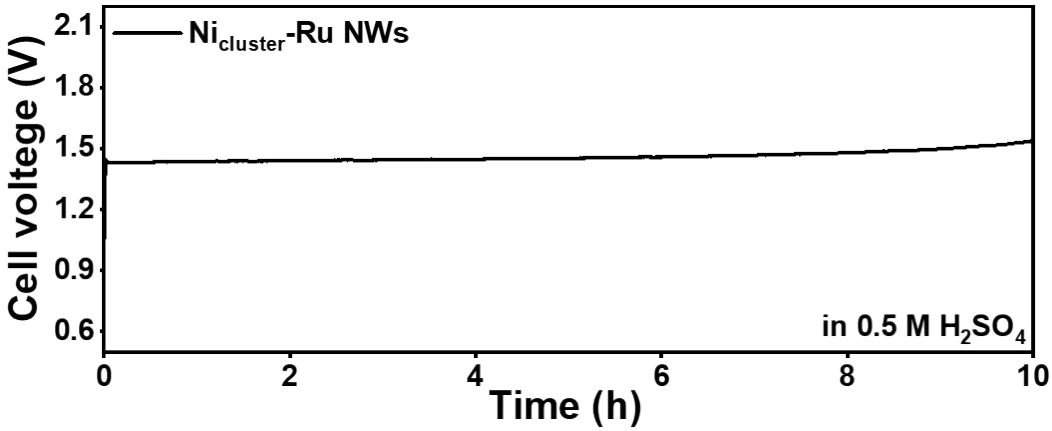

1

2 **Fig. S20.** Chronopotentiometry curve of $Ni_{cluster}$-Ru NWs in 0.5 M H_2SO_2 at 5 mA cm^{-2}.

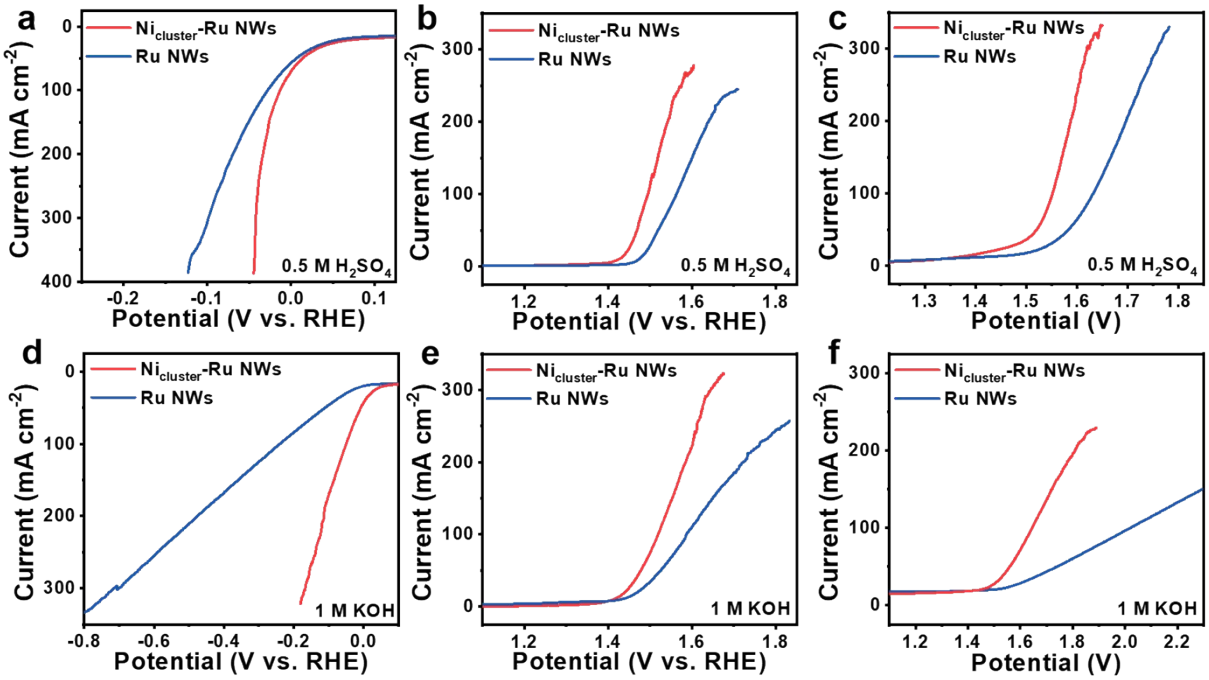

Fig. S21. Polarization curves of $Ni_{cluster}$-Ru NWs and Ru NWs loading on carbon paper (1 cm^2) for (**a, d**) HER, (**b, e**) OER and (**c, f**) overall water splitting of $Ni_{cluster}$-Ru NWs in (**a, b, c**) 0.5 M H_2SO_4 and (**d, e, f**) 1 M KOH.

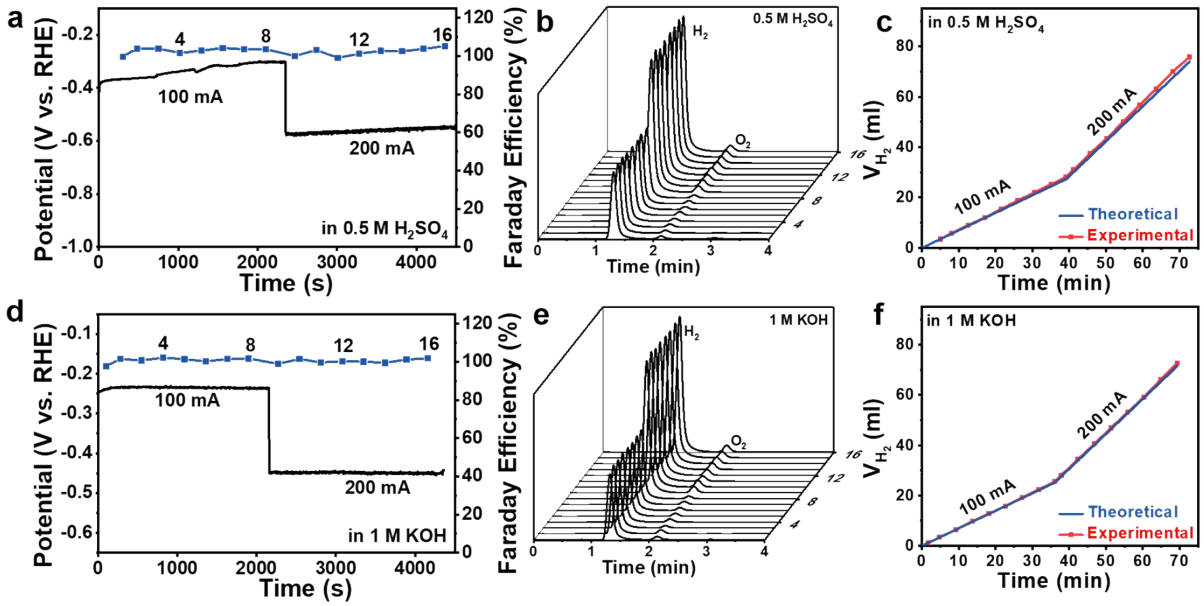

Fig. S22. (**a, d**) Faraday efficiencies, (**b, e**) GC spectra and (**c, f**) theoretical and experimental data of $Ni_{cluster}$-Ru NWs (loading on carbon paper, 1 cm^2) in (**a, b, c**) 0.5 M H_2SO_4 and (**d, e, f**) 1 M KOH.

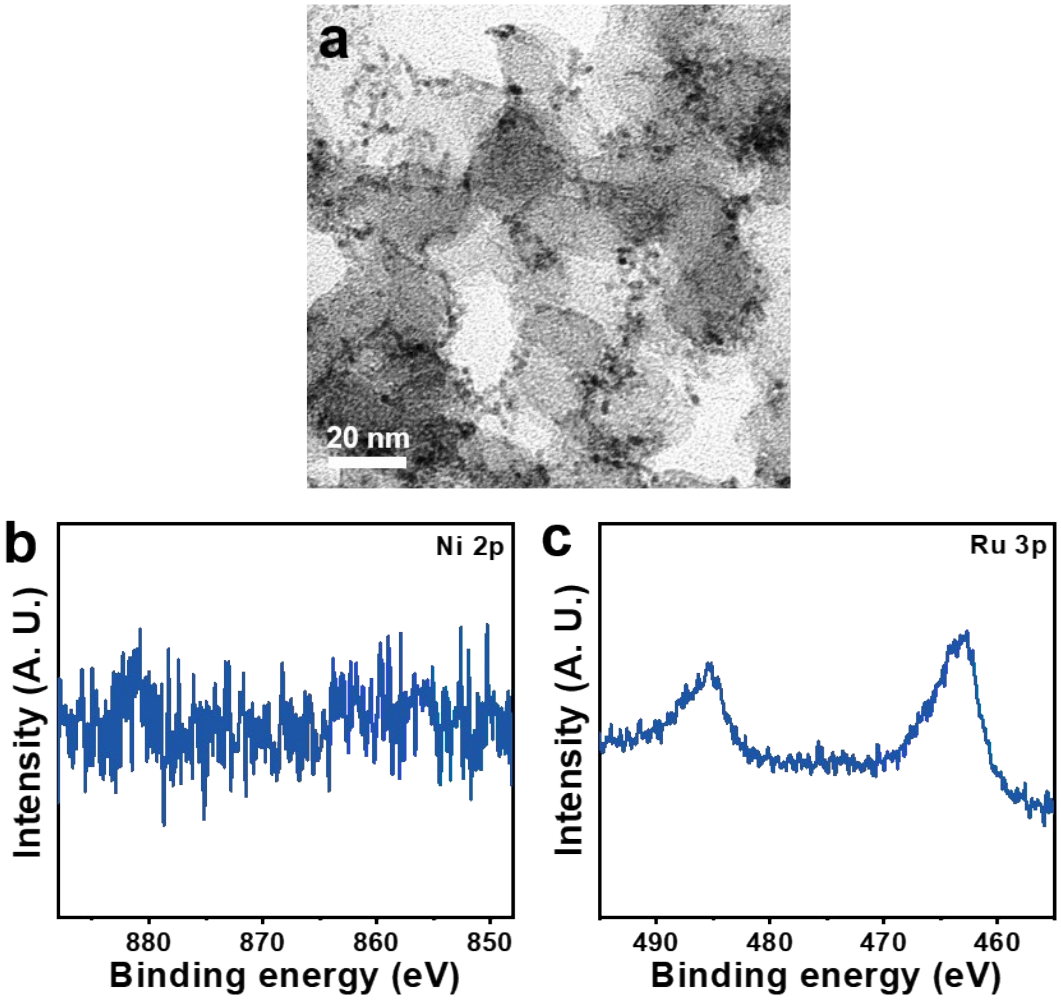

Fig. S23. (**a**) TEM image, (**b**) Ni 2p and (**c**) Ru 3p XPS spectra of $Ni_{cluster}$-Ru NWs after stability tests.

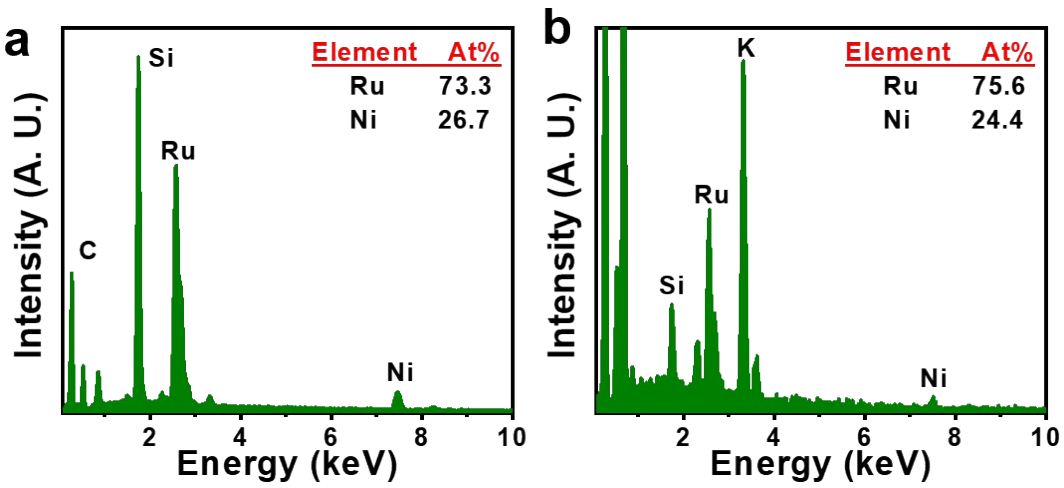

Fig. S24. EDS analyses of (**a**) as-prepared Ni-Ru NWs and (**b**) Ni-Ru NWs treated in 1 M KOH for 12 h.

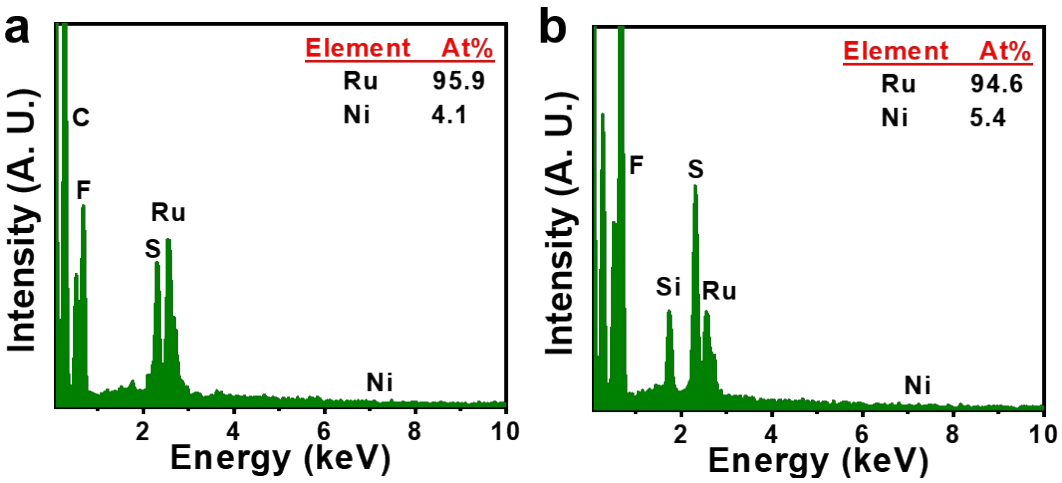

Fig. S25. EDS analyses of $Ni_{cluster}$-Ru NWs after (**a**) HER and (**b**) OER tests in 0.5 M H_2SO_4.

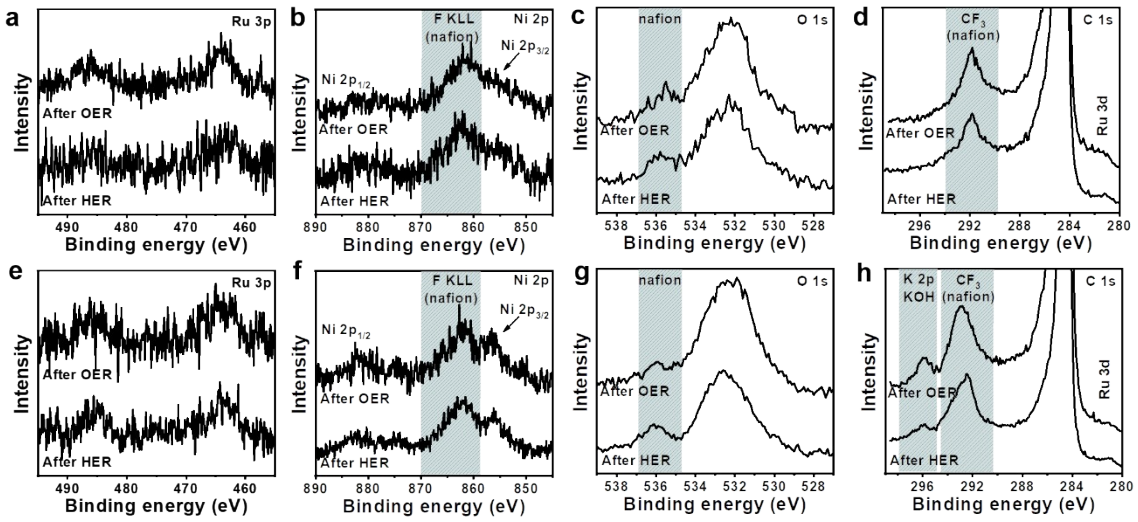

Fig. S26. (**a, e**) Ru 3p, (**b, f**) Ni 2p, (**c, g**) O 1s and (**d, h**) C 1s XPS spectra of $Ni_{cluster}$-Ru NWs after stability tests in (**a, b, c, d**) 0.5 M H_2SO_4 and (**e, f, g, h**) 1 M KOH.

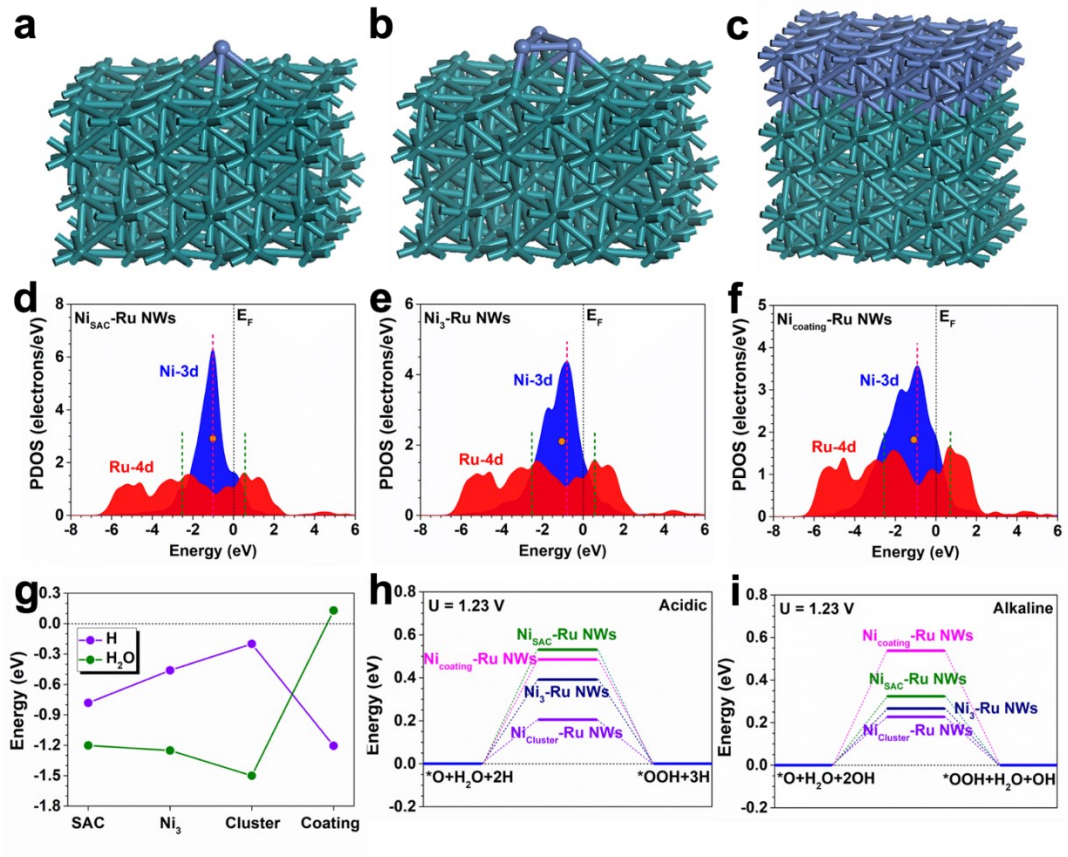

Fig. S27. The structural configurations with different size Ni cluster (**a**) Ni_{SAC}-Ru NWs, (**b**) Ni_3-Ru NWs and (**c**) $Ni_{Coating}$-Ru NWs. The PDOS of Ru NWs with different Ni cluster (**d**) Ni_{SAC}-Ru NWs, (**e**) Ni_3-Ru NWs and (**f**) $Ni_{Coating}$-Ru NWs. Orange circle represents the d-band center of Ni-*3d* bands. (**g**) The adsorption energies of H and H_2O for Ni_{SAC}-Ru NWs, Ni_3-Ru NWs, $Ni_{cluster}$-Ru NWs and $Ni_{coating}$-Ru NWs. The overpotential of OER for Ni_{SAC}-Ru NWs, Ni_3-Ru NWs, $Ni_{cluster}$-Ru NWs and $Ni_{coating}$-Ru NWs under (**h**) acidic media and (**i**) alkaline media.

We have also carried out additional calculations on the varied size of the cluster to observe the change of characteristics. As shown in **Fig. S27a-c**, we have constructed three different material systems based on the size of the Ni nanocluster. For the Ni Single-atom catalysts (SAC), the local structures of Ru NWs are barely affected. However, this structure will face realistic synthesis issues during experiments since it is highly possible to form Ni atomically doped Ru-NWs rather than Ni SAC supported by Ru NWs. As the cluster size further increases, the structure of Ru NWs will be affected more evidently. The size influences on the electronic structure are also noted in **Fig. S27d-f**. For the SAC Ni, the sharp 3d orbitals are located near E_V-1.01 eV. However, the interactions between Ni and Ru are limited, which may lead to instability during electrocatalysis (**Fig. S27d**). As the nanocluster becomes larger,

the Ni-3*d* orbitals become much broader with lower electron density. The dominant peak of Ni-3*d* orbitals upshift slightly to E_V-0.75 eV with improved electroactivity due to the stronger interactions with Ru-4*d* bands. Meanwhile, the pinning effect on Ni-3*d* bands is also noted in both Ni_3-Ru NWs and $Ni_{cluster}$-Ru NWs, which supports a much improved stability of Ni during the electrocatalysis (**Fig. S27e**). When the Ni cluster becomes too large and becomes the Ni coating, we notice that the dominant peak of Ni-3*d* bands downshifts to E_V-0.90 eV, indicating a lower electroactivity. Meanwhile, as the Ni-3*d* becomes broader, the pinning effect by Ru NWs is also much weakened, leading to lower electroactivity and stability (**Fig. S27f**). Then, the adsorption energies also demonstrate the supportive results to the electronic structures. For HER in the acidic media, the optimal value of proton binding is noted in $Ni_{cluster}$-Ru NWs, supporting the overbinding effect in other samples. Meanwhile, the strongest H_2O binding energies further guarantee the efficient water dissociation of both HER and OER in the alkaline environment (**Fig. S27g**). As confirmed by **Fig. 6d-e**, the rate-determining step locates at the conversion from [*O] to [*OOH], which determines the overpotential of the OER. The overpotential shows that $Ni_{cluster}$-Ru NWs display the lowest overpotential in both acidic and alkaline environments, which are consistent with the electronic structure and binding energies (**Fig. S27h-i**). Therefore, we have investigated the electroactivity of different size Ni cluster on Ru NWs, which further confirm that $Ni_{cluster}$-Ru NWs is the optimal electrocatalyst from both electronic and energetic perspectives.

S3. Tables

Table S1. Structural parameters of $Ni_{cluster}$-Ru NWs, NiO and Ni foil extracted from the EXAFS fitting (S_0^2 = 0.823).

Sample	Scattering pair	CN	R (Å²)	σ² (10^{-3} Å²)	ΔE_0 (eV)	R factor
$Ni_{cluster}$-Ru NWs	**Ni-Ni/Ru**	**6.88 ± 1.52**	**2.49 ± 0.012**	**5.2 ± 1.5**	**1.37 ± 1.5**	**0.0107**
NiO	Ni-Ni	12*	2.96 ± 0.009	6.1 ± 1.2	7.48 ± 3.20	0.0103
	Ni-O	6*	2.07 ± 0.022	5.1 ± 3.0	-3.25 ± 3.86	
Ni foil	Ni-Ni	12*	2.48 ± 0.007	6.0± 1.0	6.83 ± 1.38	0.0158

Note: S_0^2 is the amplitude reduction factor (obtained by the fitting of Ni foil and NiO bulk); CN is the coordination number; R is interatomic distance (the bond length between Ni central atoms and surrounding coordination atoms); σ^2 is Debye-Waller factor (a measure of thermal and static disorder in absorber-scatterer distances); ΔE_0 is edge-energy shift (the difference between the zero kinetic energy value of the sample and that of the theoretical model); R factor is used to value the goodness of the fitting.

*These values were fixed during the EXAFS fitting, based on the known structures of Ni metal and bulk NiO.

Table S2. The comparison of TOF values and mass activity performances of $Ni_{cluster}$-Ru NWs and various reported HER electrocatalysts (at 10 mA cm^{-2}).

Electrocatalyst	Electrolyte	TOF (H_2 s^{-1})	Mass activity (A g^{-1}_{Ru})	Reference
$Ni_{cluster}$-Ru NWs	1 M KOH	**8.95 (@ 50 mV)**	**1417 (@ 50 mV)**	**This work**
	0.5 M H_2SO_4	**4.58 (@ 50 mV)**	**328.3 (@ 50 mV)**	
Ru@C_2N	1 M KOH	1.66 (@ 50 mV)	244.5 (@ 34.8 mV)	*Nat. Nanotechnol.* **2017**, *12*, 441-446
	0.5 M H_2SO_4	1.95 (@ 50 mV)	244.5 (@ 35.5 mV)	
$RuIrO_x$	1 M KOH	-	1000 (@ 13 mV)	*Nat. Commun.* **2019**, *10*, 4875
	0.5 M H_2SO_4		1000 (@ 12 mV)	
Pt-Ni ASs	1 M KOH	18.63 (@ 50 mV)	1764.7 (@ 53.8 mV)	*Adv. Mater.* **2018**, 1801741
Commercial Pt/C	1 M KOH	1.62 (@ 50 mV)	588.2 (@ 61.5 mV)	*Adv. Mater.* **2018**, 1801741

Table S3. The comparison of TOF values and mass activity performances of $Ni_{cluster}$-Ru NWs and various reported OER electrocatalysts.

Electrocatalyst	Electrolyte	TOF (H_2 s^{-1})	Mass activity (A g^{-1}_{Ru})	Reference
$Ni_{cluster}$-Ru NWs	1 M KOH	**1.645 (@ 250 mV)**	**521.3 (@ 250 mV)**	**This work**
	0.5 M H_2SO_4	**4.043 (@ 250 mV)**	**593.2 (@ 250 mV)**	
Amorphous Ir nanosheets	0.1 M $HClO_4$	0.16 (@ 300 mV)	221.8 (@ 300 mV)	*Nat. Commun.* **2019**, *10*, 4855
Amorphous Li-IrO_x	0.5 M H_2SO_4	~0.32 (@ 300 mV)	~100 (@ 290 mV)	*J. Am. Chem. Soc.* **2019**, *141*, 3014-3023
IrO_2/GCN	0.5 M H_2SO_4	~0.07 (@ 320 mV)	1280 (@ 370 mV)	*Angew. Chem. Int. Ed.* **2019**, *131*, 12670-12674
IrO_x-Ir	0.5 M H_2SO_4	~0.07 (@ 240 mV)	~105 (@ 320 mV)	*Angew. Chem. Int. Ed.* **2016**, *55*, 742-746

Table S4. The comparison of the HER, OER, and overall water splitting performances of $Ni_{cluster}$-Ru NWs and various reported bifunctional catalysts (at 10 mA cm^{-2}).

Catalyst	Electrolyte	HER performance (mV)	OER performance (V)	Water splitting (V)	References
$Ni_{cluster}$-Ru NWs	**0.5 M H_2SO_4**	**20**	**1.435**	**1.454**	**This work**
	0.05 M H_2SO_4	**26**	**1.437**	**1.449**	
	0.1 M KOH	**19**	**1.440**	**1.454**	
	1 M KOH	**17**	**1.424**	**1.442**	
a-$RuTe_2$ PNRs	0.5 M H_2SO_4	33	1.475	1.52	*Nat. Commun.* **2019**, *10*, 5692
	1 M KOH	36	1.515	-	
$RuIrO_x$	0.5 M H_2SO_4	12	1.463	1.45	*Nat. Commun.* **2019**, *10*, 4875
	1 M KOH	13	1.48	1.47	
Ni-Fe NPs	1 M KOH	46	1.44	1.47	*Nat. Commun.* **2019**, *10*, 5599
NiFe-MOF	0.1 M KOH	134	1.47	1.55	*Nat. Commun.* **2017**, *8*, 15341
2.5H-PHNCMs	1 M KOH	70	1.465	1.44	*Nat. Commun.* **2017**, *8*, 15377
$NiFeO_x$/CFP	1 M KOH	88	1.51 (200 mA cm^{-2})	1.55	*Nat. Commun.***2015**, *6* 7261
CoP/NCNHP	1 M KOH	115	1.54	1.64	*J. Am. Chem. Soc.* **2018**, *140*, 2610-2618
Co_1Mn_1CH/NF	1 M KOH	180	1.524 (30 mA cm^{-2})	1.68	*J. Am. Chem. Soc.* **2017**, *139*, 8320-8328
MoS_2/Ni_3S_2	1 M KOH	110	1.448	1.56	*Angew. Chem. Int. Ed.* **2016**, *55,* 6702-6707
$NiCo_2O_4$	1 M KOH	110	1.52	1.65	*Angew. Chem. Int. Ed.* **2016**, *55,* 6290-6294
NiSe/NF	1 M KOH	96	1.5 (20 mA cm^{-2})	1.63	*Angew. Chem. Int. Ed.* **2015**, *54,* 9351-9355
h-PNRO/C	0.1 M $HClO_4$	29.6	1.469	1.524	*Adv. Mater.* **2019**, *31*, 1805546

Co-RuIr	0.1 M $HClO_4$	14	1.465	1.52	*Adv. Mater.* **2019**, *31*, 1900510
NiFeRu-LDH	1 M KOH	29	1.455	1.52	*Adv. Mater.* **2018**, *30*, 1706279
IrCoNi/CFP	0.1 M $HClO_4$ 0.5 M H_2SO_4	33 68	1.533 1.539	- 1.56 (2 mA cm^{-2})	*Adv. Mater.* **2017**, *29,* 1703798
Co-N_x|P-GC/FEG	1 M KOH	260	1.55	1.60	*Adv. Mater.* **2017**, *29,* 1604480
NiFe LDH-NS@DG10	1 M KOH 0.05 M H_2SO_4 0.1 M KOH 1 M KOH	300 96 119 39	1.44 1.542 1.624 1.534	1.5 (20 mA cm^{-2}) ~1.63 ~1.73 ~1.57	*Adv. Mater.* **2017**, *29,* 1700017
Porous MoO_2	1 M KOH	27	1.49	1.53	*Adv. Mater.* **2016**, *28,* 3785-3790
Ru NWs-Ir NWs	1 M KOH	38 (Ir NWs)	1.454 (Ru NWs)	1.47	*Adv. Funct. Mater.* **2018**, *28*, 1803722
Co/NBC-900	1 M KOH	117	1.532	1.68	*Adv. Funct. Mater.* **2018**, *28*, 1801136
IrNi NCs	0.5 M H_2SO_4 0.1 M $HClO_4$	32 (20 mA cm^{-2}) 21 (20 mA cm^{-2})	1.55 1.51	1.58 -	*Adv. Funct. Mater.* **2017**, *27,* 1700886
Ni/NiP	1 M KOH	130	1.5 (30 mA cm^{-2})	1.61	*Adv. Funct. Mater.* **2016**, *26,* 3314-3323
$NiCo_2S_4$ NW/NF	1 M KOH	210	1.49	1.63	*Adv. Funct. Mater.* **2016**, *26,* 4661-4672
$Ni_{0.51}Co_{0.49}P$	1 M KOH	82	1.469	1.57	*Adv. Funct. Mater.* **2016**, *26*, 7644-7651
Co_3Se_4/CF	1 M KOH	179	-	1.59	*Adv. Energy Mater.* **2017**, *7*, 1602579
Ni-Co-P HNBs	1 M KOH	107	1.50	1.62	*Energy Environ. Sci.* ***2018**, 11, 872-880*
Cu@NiFe LDH	1 M KOH	116	1.429	1.54	*Energy Environ. Sci.* **2017**, *10,* 1820-1827
Ru_3Ni_3 NAs	0.5 M H_2SO_4 0.05 M H_2SO_4 0.1 M KOH 1 M KOH	39 96 119 39	1.482 1.542 1.624 1.534	1.51 ~1.63 ~1.73 ~1.57	*iScience* **2019**, *11,* 492-504
NC-CNT/CoP	0.5 M H_2SO_4 1 M KOH	62 120	1.58 1.47	1.66 1.63	*J. Mater. Chem. A,* **2018**, *6,* 9009-9018
$NiAl_6P$/NF	0.5 M H_2SO_4 1 M KOH	35 80	1.486 1.472	1.52 1.55	*J. Mater. Chem. A,* **2018**, *6,* 9420-9427
IrW nanobranches	0.1 M $HClO_4$ 0.1 M KOH	16 39	1.501 1.521	1.58 1.60	*Nanoscale,* **2019**, *11,* 8898-8905
Ir WMWs	0.1 M $HClO_4$ 0.5 M $HClO_4$	11.3 15.4	1.513 1.50	1.62 -	*Nanoscale* **2018**, *10*, 1892-1897

Table S5. EDS analyses of $Ni_{cluster}$-Ru NWs and Ni-Ru NWs before and after electrochemical measurements in different electrolytes.

Samples	Initial (%)	In 0.5 M H_2SO_4 (%)		In 1 M KOH (%)	
		After HER	After OER	After HER	After OER
Ni-Ru NWs	73.3 : 26.7	-	-	-	-
$Ni_{cluster}$-Ru NWs	94.0 : 6.0	95.9 : 4.1	94.6 : 5.4	93.8 : 6.2	96.0 : 4.0

Table S6. Ni contents in $Ni_{cluster}$-Ru NWs measured by ICP-OES after electrochemical measurements in different electrolytes.

Samples	Initial (%)	In 0.5 M H_2SO_4 (%)		In 1 M KOH (%)	
		After HER	After OER	After HER	After OER
$Ni_{cluster}$-Ru NWs	6.9	6.2	2.9	6.2	5.0

References

1. B. Ravel, M. Newville, *J Synchrotron Radiat* **2005**, *12*, 537-541.
2. M. Zhu, Q. Shao, Y. Qian, X. Huang, *Nano Energy* **2019**, *56*, 330-337.
3. J. Ding, Y. Zhou, Y. Li, S. Guo, X. Huang, *Chem. Mater.* **2016**, *28*, 2074-2080.
4. Q. Shao, Y. Wang, S. Yang, K. Lu, Y. Zhang, C. Tang, J. Song, Y. Feng, L. Xiong, Y. Peng, Y. Li, H. L. Xin, X. Huang, *ACS Nano* **2018**, *12*, 11625-11631.
5. I. A. Vladimir, F. Aryasetiawan, A. I. Lichtenstein, *J. Phys. Condens. Matter* **1997**, *9*, 767.
6. S. J. Clark, M. D. Segall, C. J. Pickard, P. J. Hasnip, M. I. J. Probert, K. Refson, M. C. Payne, *zkri* **2005**, *220*, 567.
7. N. Marzari, D. Vanderbilt, M. C. Payne, *Phys. Rev. Lett.* **1997**, *79*, 1337-1340.
8. M. I. J. Probert, M. C. Payne, *Phys. Rev. B* **2003**, *67*, 075204.
9. L. Kleinman, D. M. Bylander, *Phys. Rev. Lett.* **1982**, *48*, 1425-1428.
10. S. G. Louie, S. Froyen, M. L. Cohen, *Phys. Rev. B* **1982**, *26*, 1738-1742.
11. I. Grinberg, N. J. Ramer, A. M. Rappe, *Phys. Rev. B* **2000**, *62*, 2311-2314.
12. A. M. Rappe, K. M. Rabe, E. Kaxiras, J. D. Joannopoulos, *Phys. Rev. B* **1990**, *41*, 1227-1230.
13. J. Mahmood, F. Li, S. M. Jung, M. S. Okyay, I. Ahmad, S. J. Kim, N. Park, H. Y. Jeong, J. B. Baek, *Nat. Nanotechnol.* **2017**, *12*, 441-446.